

Control of frequency chirp in nanosecond-pulsed laser spectroscopy.

2. A long-pulse optical parametric oscillator for narrow optical bandwidth

Richard T. White, Yabai He, and Brian J. Orr

Centre for Lasers and Applications, Macquarie University, Sydney, NSW 2109, Australia

Mitsuhiko Kono and K. G. H. Baldwin

Research School of Physical Sciences and Engineering, Australian National University, Canberra, ACT 0200, Australia

Received January 6, 2004; revised manuscript received March 29, 2004; accepted April 5, 2004

An injection-seeded optical parametric oscillator (OPO) based on periodically poled KTiOPO_4 is pumped at 532 nm by relatively long (~ 27 -ns) pulses from a specially constructed Nd:YAG laser. This pulsed OPO system generates continuously tunable, single-longitudinal-mode output at signal wavelengths near 842 nm, which is suitable for high-resolution spectroscopy. Optical-heterodyne measurements show that chirp in the instantaneous frequency of the pulsed OPO signal output radiation increases linearly as the seed frequency is detuned from the free-running (unseeded) OPO frequency. The frequency chirp can be maintained below 10 MHz, which is substantially less than the Fourier-transform-limited optical bandwidth (17.5 MHz full width at half-maximum for a 25-ns OPO signal pulse) and is insensitive to variation of the fluence of the pump radiation. The effects of detuning the OPO cavity length from resonance with the seed frequency and the onset of partially seeded OPO operation are also investigated. © 2004 Optical Society of America
OCIS codes: 040.2840, 120.5050, 190.2620, 190.4970, 300.6320.

1. INTRODUCTION

There is ongoing demand for high-performance sources of pulsed, continuously tunable coherent light, such as dye lasers and optical parametric oscillator (OPO) or optical parametric amplifier (OPA) devices, with high peak power, narrow optical bandwidth, and pulse durations in the range of 5–50 ns. For instance, various applications in high-resolution laser spectroscopy require such nanosecond- (ns-) pulsed sources either because their continuous-wave (cw) counterparts have insufficient power or because mode-locked and free-electron lasers (pulse duration, < 1 ns) have too high an optical bandwidth.

Particular spectroscopic applications include those that entail efficient nonlinear-optical (NLO) wavelength conversion of coherent radiation from a tunable laser, OPO, or OPA system. Specific examples within our own areas of research interest comprise spectroscopy in the vacuum ultraviolet (VUV; approximately 105–180 nm) and the extreme-ultraviolet (XUV; < 105 nm) regions. For instance, measurements have been made^{1–3} of the $2^1S \leftarrow 1^1S$ two-photon absorption transition of helium (He) with narrowband VUV radiation near 120.28 nm. Likewise, XUV plus ultraviolet two-photon ionization spectroscopy has been performed on molecular nitrogen (N_2),⁴ with narrowband pulsed XUV radiation at 90–100 nm used to prepare N_2 in its two lowest-energy $^1\Pi_u$ electronic manifolds. In these investigations the narrowband

pulsed VUV or XUV radiation was generated by pulsed dye amplification of narrowband continuously tunable infrared or visible light from a cw Ti:sapphire laser^{1–3} or a cw dye laser,⁴ followed by NLO harmonic upconversion. However, it has proved difficult to control instrumental line-broadening processes reliably in the case of the previously employed dye-laser pulse amplification media,^{1–3,5} so solid-state OPO or OPA and laser media are expected to be advantageous. Continuously tunable, narrowband coherent light with ns pulse duration is also required for various spectroscopic applications that entail a time-resolved molecular excitation sequence, such as our infrared–ultraviolet double-resonance studies of J -resolved, collision-induced rovibrational energy transfer in acetylene (C_2H_2).^{6–10}

In a recent publication¹¹ we reported a major advance in the techniques that are required for control of the optical bandwidth and frequency chirp characteristics of output from a single-longitudinal-mode (SLM), continuously tunable OPO system based on the quasi-phase-matched NLO medium, periodically poled KTiOPO_4 (PPKTP). This PPKTP OPO was injection seeded by a cw tunable diode laser (TDL) at a signal wavelength λ_s of ~ 842 nm and pumped at 532 nm by a SLM Nd:YAG laser with a pulse duration of ~ 8 ns. The optical phase properties of output from this form of high-performance ns-pulsed tunable OPO have been measured¹¹ by optical heterodyne (OH) techniques, in which the pulsed radiation beats against cw TDL seed radiation that has been

frequency shifted by an acousto-optic modulator (AOM). Such OH techniques were further explained and evaluated in a preceding paper.¹²

In the present paper we introduce a specially constructed SLM Nd:YAG pump laser with a long cavity to yield a full width at half-maximum (FWHM) pulse duration of ~ 27 ns (3.5 times that employed in the research reported in Ref. 11). This longer-pulse extension yields better performance than that of the 8-ns pulsed OPO that was reported previously.¹¹ The Fourier-transform (FT) limit associated with the increased OPO output pulse duration (~ 25 ns FWHM) results in a substantially reduced FT-limited optical bandwidth of ~ 17.5 MHz FWHM. Here we use OH techniques, as described in Ref. 12, to characterize the frequency chirp of the pulsed OPO output radiation, establishing chirp-minimization techniques to maintain chirp well below the FT-limited optical bandwidth. The longer-pulse OPO system is intended to serve as the first SLM tuning stage of a high-performance narrowband VUV–XUV spectroscopic system, with improved resolution and accuracy relative to earlier systems.^{1–3,5}

The structure of this paper is as follows: In Section 2 we survey operational factors that are likely to give rise to frequency-chirp effects in the output from the OPO system. Details of our apparatus design (additional to those reported in Ref. 12) are presented in Section 3. In Section 4 we present, analyze, and discuss our experimental results. Finally, in Section 5 we present some conclusions and projections for future investigations.

2. ORIGINS OF OPTICAL PARAMETRIC OSCILLATOR FREQUENCY CHIRP

Here we are specifically interested in instantaneous frequency perturbations that occur on a ns time scale in NLO media, particularly in OPOs and OPAs. Such effects are usually referred to as chirp when the changes in instantaneous frequency during a pulse are linear (or at least monotonic). There is ample literature on the optical phase dynamics for NLO interactions of ultrafast pulses in the picosecond and femtosecond regimes. However, there have been relatively few reports of such processes in the context of ns (or longer) pulses, where FT-limited optical bandwidths are smaller, permitting superior spectroscopic resolution. For ns pulses it is reasonable to simplify the treatment of NLO phase dynamics by ignoring group-velocity dispersion.

A treatment¹³ of ns-pulsed second-harmonic generation for incident light of angular frequency ω indicates that the dominant phase-perturbation contribution to second-harmonic generation comes from the NLO susceptibility $\chi^{(2)}(-2\omega; \omega, \omega)$ and its effect on the corresponding phase mismatch, Δk . This result is consistent with a finding¹⁴ that, in the picosecond regime, the phase modulation depends on Δk . Likewise, in the context of ns-pulsed OPOs and OPAs it is understood^{15,16} that phase mismatch Δk causes the amplified waves to experience a phase shift because the wave vector of the NLO polarization that produces that amplification (e.g., induced by the OPO pump wave) is not equal to that of the incident wave (e.g., the OPO signal or idler wave). It is also recognized^{15–17} that nonresonant idler (or signal) feedback can cause fre-

quency shifts in the signal (or idler) wave of a pulsed, singly resonant OPO. Our earlier study¹¹ of an 8-ns pumped OPO indicated that other chirp effects may arise through cavity pulling if the OPO cavity's resonance frequency is displaced from the injection-seeding frequency.

There have been several authoritative investigations, based on OH techniques, of the optical phase properties of pulsed, tunable coherent light from dye-laser amplifiers.^{3,13,18,19} In such dye-laser media, time-dependent changes in the gain can alter level populations, thereby producing corresponding variations in the refractive index and giving rise to phase modulation. In this paper we are concerned more with NLO media in general and with OPO or OPA media in particular, so gain-induced population changes are irrelevant and other mechanisms merit consideration.

We are particularly interested in optical phase perturbations in a NLO medium such as a single-pass optical parametric generator (OPG). In a treatment that parallels that of Gangopadhyay *et al.*¹³ we formulate possible sources of optical phase perturbations in such a medium. We consider a plane wave, $\mathbf{E}(z, t)$, which describes the electric field of linearly polarized monochromatic light propagating along the z axis:

$$\begin{aligned} \mathbf{E}(z, t) &= \mathbf{E}^0(t) \exp[i\langle\omega\rangle t + i\phi(z, t)] + \text{c.c.} \\ &= \mathbf{E}^0(t) \exp[i(\phi_0 + \langle\omega\rangle t - k(z, t)z)] + \text{c.c.}, \end{aligned} \quad (1)$$

where c.c. denotes a complex conjugate. $\mathbf{E}^0(t)$ is the electric-field amplitude vector in the x – y plane and $\phi(z, t)$ is the optical phase, relative to a value of ϕ_0 at a point $(z, t) = (0, 0)$ that we choose to be at the entrance face of the NLO crystal of the OPG. The angular frequency $\langle\omega\rangle$ of incident light is a central value that is effectively time independent; as explained in Ref. 12, the absolute value of $\langle\omega\rangle$ is not important because we are concerned only with the beat frequency between the pulsed optical field and the cw AOM-shifted TDL-seed radiation. In the case of ns-pulsed radiation, $\mathbf{E}^0(t)$ has an explicit, slowly varying time dependence; $\mathbf{E}^0(t)$ can be assumed to be real, without loss of generality. Any phase perturbations during the pulse evolution are assigned separately to $\phi(z, t)$.

Within the OPG NLO medium of length L it is necessary to integrate wave vector amplitude k in Eq. (1) to obtain a value at the NLO medium's exit face, as follows:

$$k(L, t) = (\langle\omega\rangle/cL) \int_0^L n(z, t) dz, \quad (2)$$

where c is the speed of light. Refractive index n has an explicit dependence on z and t in general; it is effectively constant during the time that a wave front takes to traverse the crystal.

For a wave as in Eq. (1), the instantaneous frequency, $f_{\text{inst}}(L, t)$, of light emerging from the OPG medium is defined^{13,20} by

$$f_{\text{inst}}(L, t) = (2\pi)^{-1} \partial \phi(L, t) / \partial t, \quad (3)$$

such that f_{inst} is zero if there are no phase perturbations. It follows from Eqs. (1) and (2) that

$$\begin{aligned} f_{\text{inst}}(L, t) &= -(2\pi)^{-1} L [\partial k(L, t) / \partial t] \\ &= -(2\pi c)^{-1} \langle \omega \rangle L [\partial n(t) / \partial t], \end{aligned} \quad (4)$$

where $n(t) = L^{-1} \int_0^L n(z, t) dz$ is averaged over the NLO medium's length L ; ϕ_0 in Eq. (1) is constant and makes no contribution to $f_{\text{inst}}(L, t)$. An optical medium with a time-dependent refractive index $n(t)$ will therefore induce a change in instantaneous frequency f_{inst} of an electromagnetic wave propagating through it, even if the incident wave is monochromatic. Such an instantaneous frequency change is a form of frequency chirp. For $z > L$, light emerging from the single-pass NLO medium propagates in air, for which k and n are time independent, so $f_{\text{inst}}(z, t)$ then contains no additional chirp contributions relative to $f_{\text{inst}}(L, t)$ as in Eq. (4).

There are several ways in which a nonzero value of $[\partial n(t) / \partial t]$ can arise in the NLO medium of an OPG within the duration of its pump and output pulses. Obvious mechanisms entail phase modulation associated with the optical Kerr effect: either self-phase modulation or cross-phase modulation, by means of the NLO susceptibilities $\chi^{(3)}(-\omega; \omega, \omega, -\omega)$ and $\chi^{(3)}(-\omega; \omega, \omega', -\omega')$, where $\omega' \neq \omega$. Cascaded $\chi^{(2)}$ interactions have also been shown²¹ to yield phase shifts at lower optical intensities than are required by their $\chi^{(3)}$ counterparts.

The foregoing treatment applies to a single-pass NLO medium, such as that of an OPG. If the NLO medium is placed inside an optical cavity (e.g., converting a single-pass OPG into an OPO), the optical phase of the output radiation is also affected by round-trip phase changes. We do not treat this phenomenon explicitly here, but we previously showed¹¹ that displacing the OPO cavity's resonance frequency from the seed frequency can result in additional cavity-pulling effects.

The above sources of frequency chirp are associated with variations in the refractive index. However, there may be other sources of frequency chirp that are independent of the optical properties of the NLO medium. For instance, perturbations in the instantaneous frequency f_{inst} of output from an OPO can also arise if the frequency of the incident light is itself time dependent. This might occur if there is frequency chirp in the pump-laser pulse, for example, from the oscillator, amplifier, or second-harmonic-generation stage of a ns-pulsed Nd:YAG laser.²² We also note suggestions²³ that the phase-matching conditions of an OPO can cause additional excursions in the signal and idler output frequencies if the pump frequency is shifted by self-phase modulation, depending on the contribution from $\chi^{(3)}(-\omega; \omega, \omega, -\omega)$.

Mechanisms such as these are capable of giving rise to the OPO frequency chirp effects that are measured in this paper. Here we aim to determine the extent and reproducibility of such phase-perturbation effects as a means of refining a high-performance pulsed laser-spectroscopic system. We do not attempt to distinguish which of several possible chirp contributions is dominant but rather to establish how frequency chirp depends on controllable OPO operational parameters. This investigation is in-

tended to provide phenomenological ways to minimize frequency chirp or to make it sufficiently reproducible to enable chirp-correction techniques (e.g., by electro-optic phase modulation⁵) to be implemented.

3. INSTRUMENTATION

Figure 1 depicts the periodically poled KTiOPO₄ (PPKTP) OPO and the system that is used to measure the instantaneous-frequency characteristics of its signal output at ~ 842 nm. The four-mirror ring OPO is similar to that described in a previous paper.¹¹ Cavity mirrors M1 and M2 have radii of curvature of 20 cm and are coated for minimum reflection at 532 nm and for 80% reflection at 800–900 nm. These two mirrors serve as output couplers; the output from M1 is used for the OH measurements, and the output from M2 is directed to a pulsed wavemeter (Burleigh 4500-1) for wavelength and spectral monitoring. The OPO cavity that contains the PPKTP NLO medium is completed by mirrors M3 and M4 (each flat and coated for high reflection at 800–900 nm); its physical round-trip distance is approximately 12 cm.

The OPO is pumped by a custom-built, frequency-doubled Nd:YAG laser (Continuum Powerlite 8000), which produces SLM pulses at a wavelength of 532 nm with a duration of 27 ns FWHM and a repetition rate of 10 Hz. In its high-beam-quality mode of operation, this laser was used to produce a maximum 532-nm output pulse energy of ~ 400 mJ with a quasi-Gaussian beam profile in the near field. Only a small fraction (~ 100 μ J) of the total pump-pulse energy is needed to pump the OPO, and the remaining energy is available for other purposes, such as pumping OPA stages to increase the signal and idler output pulse energies, as is currently under investigation.

The PPKTP crystal (1 mm \times 2 mm \times 20 mm) is mounted in a temperature-controlled oven insulated with poly-(tetrafluoroethylene) and is placed midway between mirrors M1 and M2. In the present experiments, its 9.35- μ m grating period provides a quasi-phase-matched tuning range for the free-running OPO as depicted in Fig.

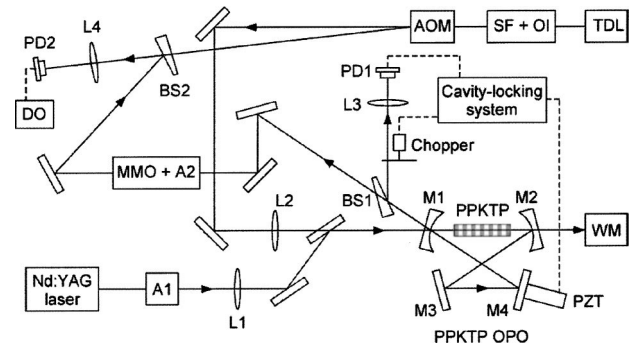


Fig. 1. Schematic of the long-pulse injection-seeded PPKTP OPO and the OH detection system: A1, A2, attenuators; BS1, BS2, beam splitters; WM, wavemeter; SF, spatial filter; OI, optical isolator; AOM, acousto-optic modulator (~ 730 -MHz); PZT, piezoelectric translator; MMO, mode-matching optics; DO, digital oscilloscope; M1–M4, cavity mirrors; TDL, tunable diode laser; PD1, PD2, photodetectors; L1–L4, lenses.

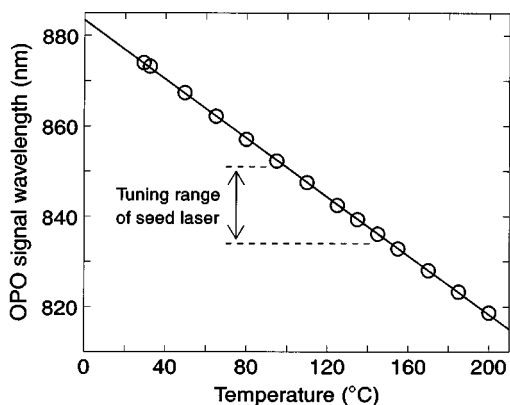


Fig. 2. Temperature dependence of the measured phase-matched wavelength λ_{free} for signal output from the free-running PPKTP OPO. The ordinate intercept is 883.4 nm, and the slope is -0.326 nm K^{-1} . The wavelength tuning range of the TDL injection seeder is 834–851 nm.

2, where the wavelength, λ_{free} , for signal output has a range of 818–875 nm with PPKTP temperatures in the range 200–25 °C.

The PPKTP OPO is injection seeded by an external-cavity, SLM TDL (New Focus 6316) with a continuous output wavelength range of 834–851 nm. This range defines the currently accessible SLM tuning range of the OPO signal output, as indicated in Fig. 2. The output of the TDL is spatially filtered, permitting better mode matching to the OPO cavity and also minimizing phase-front distortion across the beam. The spatial filter (which comprises a 50- μm -diameter pinhole and two 50-mm focal-length lenses) transmits $\sim 50\%$ of the TDL-seed light, giving $\sim 5 \text{ mW}$ of cw power at its output. Following the spatial filter, the TDL-seed light is passed through an AOM (Brimrose TEM-100-30) driven at $\sim 730 \text{ MHz}$. The zero-order beam is used to seed the OPO through mirror M1. Within each 10-Hz laser-pulse cycle the OPO resonator length is locked to the TDL-seed frequency by an intensity-dip locking system^{24,25} that comprises beam splitter BS1, a mechanical light chopper, photodetector PD1, cavity-locking electronics, and a piezoelectric translator (PZT) on cavity mirror M4 (Fig. 1).

The OPO signal output (from mirror M1) is attenuated and combined collinearly at beam splitter BS2 with the first-order frequency-shifted beam from the AOM. The combined beams are then focused onto a 1-GHz photodetector (PD2; New Focus 1601) by a 50-mm focal-length lens. The AOM conversion efficiency to the first-order beam is $\sim 15\%$, giving $\sim 0.8 \text{ mW}$ of cw power for the OH measurement. Good overlap of the wave fronts of the two beams is critical for the frequency-chirp measurements, so correct alignment and spatial overlap of the OPO pulsed light and the cw AOM-shifted TDL-seed light at photodetector PD2 is critical. The OH beat waveform generated by PD2 is digitized by a 2-GHz digital oscilloscope (Tektronix TDS794D) at 4 GSa s^{-1} , where Sa is one digital sample. The recorded beat waveforms are analyzed by the FT technique described in Ref. 12. The FT technique was chosen over the alternative direct-fit and mixer methods because its accuracy had previously been

well established^{11,12} under low-chirp conditions as in the present experiment and because a high-bandwidth ($>1\text{-GHz}$) detection and digitizing system is available to us. An 82-ns optical delay line (similar to that previously used¹²) enables the unmodulated time profile of the OPO signal pulse to be measured in a single recording by the same photodetector, PD2. Fourier transformation of a set of ten OPO pulse time profiles ($\sim 25 \text{ ns FWHM}$) yields a FT-limited optical bandwidth of $17.5 \pm 1.0 \text{ MHz FWHM}$.

4. EXPERIMENTAL RESULTS

Figure 3 shows the seeded and unseeded OPO output signal pulse energy as a function of pump-pulse energy. The OPO beam quality is very good, with M^2 measured to be ~ 1.1 . The OPO energy data are the combined energy emitted from the two output couplers. As expected, the threshold is lower for seeded operation ($19 \mu\text{J}$, compared to $27 \mu\text{J}$) but, above $\sim 40 \mu\text{J}$, the seeded curve rolls off markedly. This may be due to backconversion of the signal and idler waves to the pump wave^{15,26} or to other assorted cascaded processes such as sum-frequency generation from the pump and the OPO output waves; we have observed such effects spectroscopically. Evidence of such processes has also been seen in the form of saturation in the intensity profiles of the signal pulse near its peak.

In our previous study of a PPKTP OPO with 8-ns pump pulses,¹¹ the phase mismatch (Δk) in the optical parametric process was found to be a significant source of frequency chirp. We have investigated the effects of phase mismatch with 27-ns pump pulses by altering OPO signal wavelengths λ_s above and below the free-running wavelength, λ_{free} (841.75 nm, for a PPKTP crystal temperature of 125 °C).

Figure 4 shows $f_{\text{inst}}(t)$ curves derived by the FT technique for several values of λ_s . The pump-pulse energy used ($60 \mu\text{J}$) was twice the unseeded OPO threshold, which was observed to vary from day to day, probably associated with slight changes in pump-beam quality, in

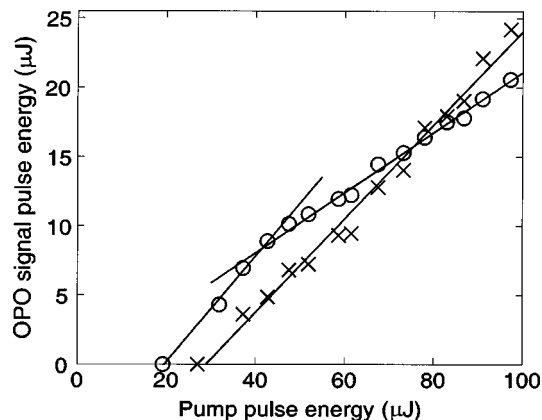


Fig. 3. Total output signal pulse energy (from both output couplers, M1 and M2) as a function of pump-pulse energy incident upon the OPO for seeded (\circ) and unseeded (\times) operation. The roll-off in the seeded curve is discussed in the text. The threshold for seeded operation is $19 \mu\text{J}$, and the slope efficiency is 38% (before roll-off) and 22% (after roll-off). The corresponding unseeded results are $27 \mu\text{J}$ and 34%, respectively.

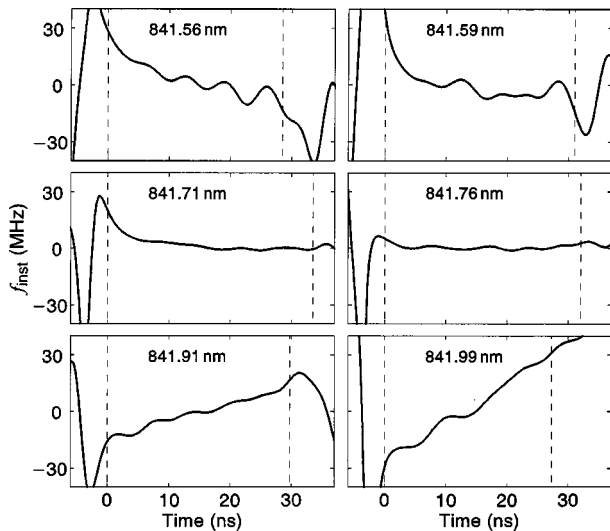


Fig. 4. Instantaneous-frequency $f_{\text{inst}}(t)$ profiles extracted by the FT algorithm for several injection-seeder wavelengths above and below λ_{free} (841.75 nm). The pump-pulse energy is twice the unseeded threshold level, and the PPKTP temperature is maintained at 125 °C. Vertical dashed lines, 10%-intensity points of the OPO pulses.

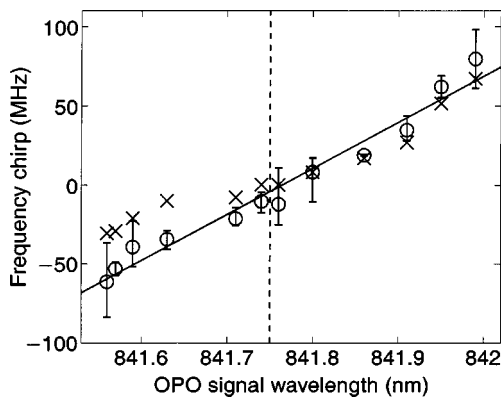


Fig. 5. Frequency chirp as a function of OPO signal wavelength λ_s for the linear-fit (\times) and the Δf_{inst} (\circ) definitions.¹² Each entry is an average of four pulse measurements as in Fig. 4, at a PPKTP temperature of 125 °C. Solid line, unweighted straight-line fit to the Δf_{inst} data points; error bars show the scatter of Δf_{inst} values that contribute to each point. The fit has a slope of $292 \pm 17 \text{ MHz nm}^{-1}$, and it predicts a minimum-chirp wavelength of 841.76 nm. Vertical dashed line, free-running signal wavelength, λ_{free} (841.75 nm).

OPO cavity alignment, or in both; its value in the context of Fig. 4 was $30 \mu\text{J}$, rather than $27 \mu\text{J}$ as in Fig. 3. The results in Fig. 4 confirm that the sign of the Δk -induced chirp is such that the instantaneous frequency of the OPO signal pulse evolves toward the free-running OPO frequency, with the magnitude of the chirp dependent on the size of the phase mismatch.^{11,13,14,27}

As explained in Ref. 12, we previously¹¹ introduced two distinct (but approximately equivalent) measures of the overall chirp within a given time interval: either the difference Δf_{inst} between maximum excursions of f_{inst} or the slope of a linear fit to the f_{inst} profile. These two measures of overall chirp, based on data such as those of Fig. 4, are plotted in Fig. 5 as a function of OPO signal wave-

length λ_s . A straight-line least-squares fit to the Δf_{inst} data yields zero chirp at λ_{free} (within the 0.01-nm uncertainty of the wavemeter reading). The slope of the fit is $292 \pm 17 \text{ MHz nm}^{-1}$, which is similar to the corresponding value ($261 \pm 9 \text{ MHz nm}^{-1}$) from our previous report of a PPKTP OPO with 8-ns pump pulses.¹¹

The span of wavelengths in Fig. 5 corresponds approximately to the full range of λ_s values over which seeding is effective. At a constant temperature, the seeding range is governed by the phase-matching bandwidth of the PPKTP crystal (predicted to be 0.66 nm for a perfect quasi-phase-matched grating). The seeding range also decreases as the pulse duration increases because a longer pulse duration allows more time for the OPO to evolve from SLM seeded operation to broad-band, free-running operation; such a process is enhanced near the wings of the seeding range.

Figure 6 shows ten $f_{\text{inst}}(t)$ curves for OPO operation at λ_{free} and with a pump-pulse energy that corresponds to twice the unseeded threshold, as in Figs. 4 and 5. During the majority of the OPO pulse, the variation in f_{inst} is small. The fluctuations or oscillations in these curves vary sporadically from pulse to pulse. Excursions near each pulse's leading edge contribute to the chirp may be an artifact of the FT algorithm (e.g., as in Fig. 3 of Ref. 12). Whereas the chirp effects depicted in Fig. 4 are predominantly linear, the higher ordinate resolution of Fig. 6 gives some indication of quadratic or higher-order chirp contributions of not more than 5 MHz.

Within the 10%-intensity range of the OPO signal pulse, Fig. 6 yields a mean unsigned overall chirp $\langle |\Delta f_{\text{inst}}| \rangle$ of $11 \pm 3 \text{ MHz}$. However, this choice of intensity range is somewhat arbitrary; it is often more realistic (e.g., in OPO applications that entail subsequent NLO wavelength conversion) to confine evaluation of the overall chirp to the central, more intense portion of the OPO pulse profile. Within the 50%-intensity range of Fig. 6, the mean unsigned overall chirp $\langle |\Delta f_{\text{inst}}| \rangle$ is reduced to $7 \pm 2 \text{ MHz}$. This OPO system therefore exhibits extremely low frequency chirp relative to many comparable pulsed lasers used in high-resolution

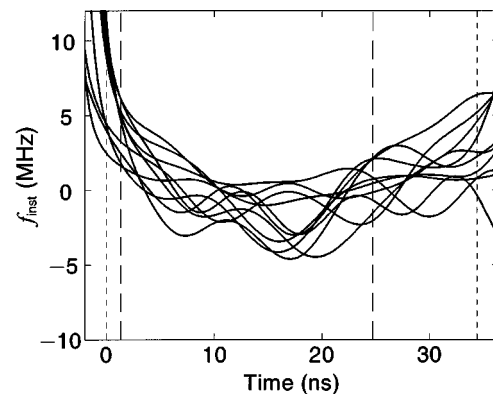


Fig. 6. Set of ten $f_{\text{inst}}(t)$ profiles for seeded OPO operation at λ_{free} (841.75 nm at a PPKTP temperature of 125 °C) and pumped at twice the unseeded threshold. Vertical short- and long-dashed lines, 10%- and 50%-intensity points for which the mean unsigned overall chirp values $\langle |\Delta f_{\text{inst}}| \rangle$ are 11 ± 3 and $7 \pm 2 \text{ MHz}$, respectively. Absolute-frequency scatter (amounting to $\pm 9 \text{ MHz}$) for these pulses is not shown.

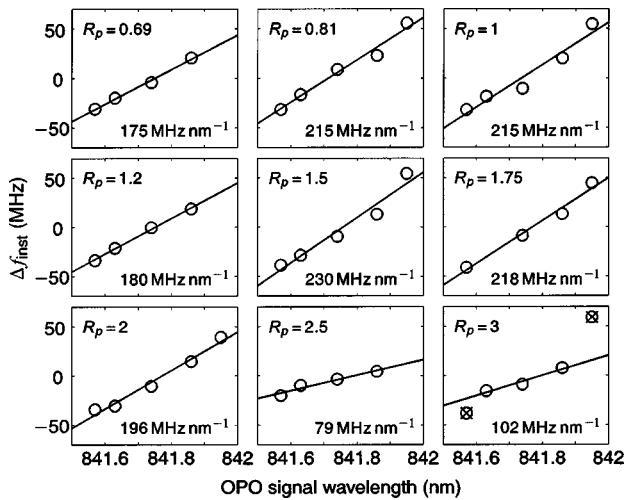


Fig. 7. Δf_{inst} as a function of OPO signal wavelength λ_s for several pump-pulse energies, with ratio R_p ranging from 0.69 to 3 times the threshold for the unseeded PPKTP OPO. Solid lines, straight-line fits to the data. In all cases these lines predict a minimum-chirp wavelength of 841.76 nm, virtually identical to $\lambda_{\text{free}} = 841.75 \pm 0.01$ nm. Two extreme data points with $R_p = 3$ (marked \times) have been rejected, as explained in the text.

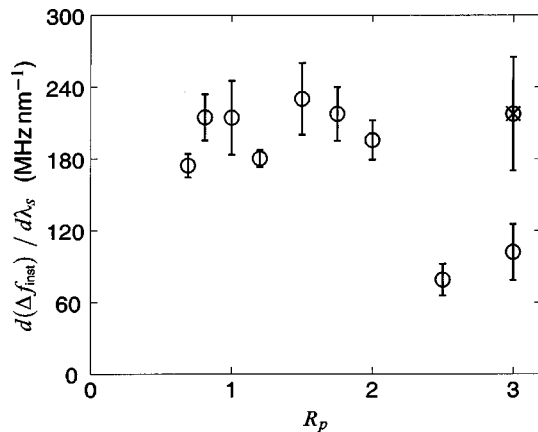


Fig. 8. Slope $d(\Delta f_{\text{inst}})/d\lambda_s$ of straight-line least-squares fits to the Δf_{inst} signal-wavelength plots in Fig. 7 plotted against pump-pulse energy ratio R_p . An error bar indicates the standard deviation of each slope fit. The two different data points for $R_p = 3$ are explained in the text.

spectroscopy.^{1-3,12,17,18,28} There are few previous reports of frequency chirp of 10 MHz or less measured in ns-pulsed coherent light sources, namely, dye-amplified dye lasers that use carefully selected dye mixtures^{29,30} and a chirp-compensated alexandrite laser.³¹ The good chirp reproducibility indicated in Fig. 6 shows promise for active chirp-compensation techniques, e.g., use of electro-optic phase modulators.⁵

Most sources of chirp (e.g., Δk , self-phase modulation) are expected to depend on the pump laser's power density.^{14,32} Figure 7 shows the extracted chirp, Δf_{inst} , as a function of signal wavelength λ_s for several values of the ratio R_p of the pump-pulse energy to the unseeded PPKTP OPO threshold (32 μJ in this set of measurements). Two extreme data points with $R_p = 3$ (marked \times) have been rejected from the fit shown in Fig. 7, owing to the

onset of partially seeded operation when λ_s is widely separated from λ_{free} for $R_p > 2$ (as is further discussed below).

Straight-line least-squares fits to each set of data in Fig. 7 yield minimum-chirp wavelengths that are independent of the pump-pulse energy and equal to λ_{free} (within the 0.01-nm uncertainty of the pulsed wavemeter). Figure 8 shows the slope $d(\Delta f_{\text{inst}})/d\lambda_s$ of straight-line fits to the data in Fig. 7 as a function of pump-pulse energy ratio R_p . Two different data points are shown for $R_p = 3$: one from the fit in Fig. 7 and the other (marked \times , with a larger error bar) from a fit that includes all five $R_p = 3$ data points plotted in Fig. 7. The former fit (from which extreme $R_p = 3$ data points have been rejected) suggests that there is a roll-off effect in $d(\Delta f_{\text{inst}})/d\lambda_s$, which may be due to residual partially seeded operation that is otherwise undetected. At the relatively low peak powers of the ~ 27 -ns pump pulses employed here, the overall chirp Δf_{inst} does not increase significantly with increasing pump-pulse energy. Our previous (less-detailed) studies of a PPKTP OPO pumped by 8-ns pulses¹¹ indicated that Δf_{inst} "increases with pump-pulse energy, consistent with phase perturbations arising from nonlinear processes."

Detuning the resonance frequency of the PPKTP OPO cavity from the TDL-seed frequency results in appreciable frequency-chirp effects if TDL-seed wavelength λ_s is widely separated from the free-running OPO wavelength λ_{free} [e.g., as observed in our previous research with short ~ 8 -ns pump pulses, $\lambda_s = 841.41$ nm, and $\lambda_{\text{free}} = 841.56$ nm (Ref. 11)]. In our current study of a virtually identical PPKTP OPO with longer-pulse (27-ns) pumping, seeded signal wavelength λ_s was set to coincide with λ_{free} at 841.70 nm to produce minimum chirp; no frequency-chirp contribution from cavity-resonance detuning is then discernible. We infer that the cavity-pulling type of frequency chirp previously observed¹¹

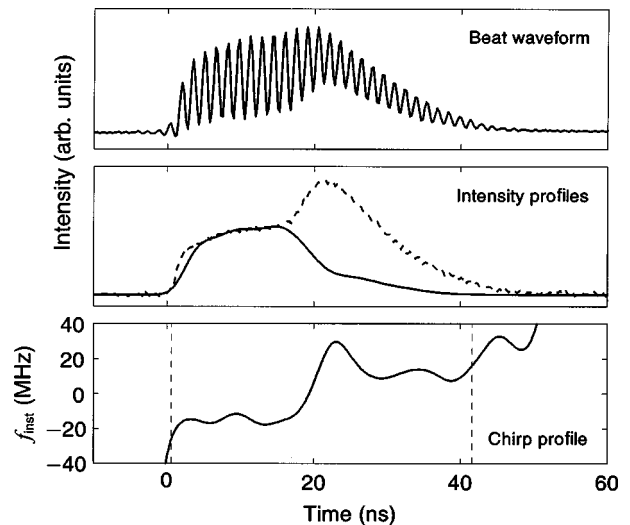


Fig. 9. Partially seeded behavior in the signal output from the long-pulse PPKTP OPO system pumped at three times the unseeded threshold ($R_p = 3$). Top, raw OH beat waveform. Center, OPO signal intensity profiles, raw (dashed curve) and reconstructed narrowband component (solid curve). Bottom, f_{inst} profile extracted with the FT algorithm; vertical dashed lines, 10% raw-intensity limits.

arises from the nonzero value of Δk that depends on the separation between λ_s and λ_{free} . Such behavior in the long-pulse OPO may also be partly attributable to the longer buildup time that is available for the OPO output wavelength to change from its (initially) seeded value to its (final) cavity-determined value.²⁴

Figure 9 shows additional measurements related to the pulse dynamics of signal output from the injection-seeded PPKTP OPO system that help us to understand some of the anomalies observed in the context of Figs. 7 and 8. Here the TDL-seeded signal wavelength λ_s is set at 841.95 nm, relatively remote from the 841.76-nm free-running signal wavelength λ_{free} for the PPKTP OPO at 125 °C. Such a wide frequency separation (2.7 cm⁻¹; 80 GHz) between λ_s and λ_{free} causes a lapse in pure SLM injection-seeded OPO operation later in the long (27-ns FWHM) pump pulse, as other free-running OPO modes build up. We therefore attribute the behavior illustrated in Fig. 9 to partially seeded OPO operation. The topmost part of the figure shows the raw modulated waveform that is recorded by the OH photodetector (PD2; Fig. 1) when the OPO is pumped at three times the unseeded threshold (32 μJ in these measurements). The OH beat oscillations associated with chirp of the SLM injection-seeded output are regularly spaced, but their contrast decreases and the intensity profile on which they are superimposed increases markedly from ~ 18 ns onward. The intensity-profile anomaly is more clearly shown in the middle of Fig. 9, where the raw, unmodulated signal intensity profile (dashed curve, measured by PD2 after an 82-ns delay) is compared with the corresponding SLM component reconstructed from the OH beat modulation (solid curve). The difference between these two curves indicates how the spectral purity³³ of the pulse evolves in time. The bottom of Fig. 9 shows the instantaneous-frequency (f_{inst}) profile extracted by use of the FT algorithm.

Corresponding measurements have been made with lower pump-pulse energies. The free-running broadband component is still evident with $R_p = 2.5$, although it is less pronounced and appears ~ 5 ns later than in Fig. 9. There is no obvious broadband component with $R_p = 2$, (similar to the bottom of Fig. 4). However, it is possible that additional unseeded OPO modes may occur without being directly observed at lower values of $|\lambda_s - \lambda_{\text{free}}|$ and R_p and (as suggested above) that this may account for the roll-off effect in Fig. 8.

Competition between seeded and unseeded outputs was previously observed in our laboratory³⁴ with a birefringently phase-matched β -barium borate OPO pumped at 355 nm with a free-running optical bandwidth of ~ 7 cm⁻¹ (~ 210 GHz); the center-spot fringe amplitude and contrast transmitted by a 1-cm⁻¹ (30-GHz) free-spectral-range Fabry–Perot etalon vary markedly as the seed radiation (at ~ 538 nm, from a pulsed dye-laser) is tuned a few wave numbers (inverse centimeters) away from the free-running OPO wavelength λ_{free} . Other observations of the onset of broadband unseeded operation in dispersed β -barium borate OPO output radiation, as the phase-matching angle is varied stepwise to shift λ_{free} away from the (seeded) signal wavelength, λ_s , have also been reported^{34–36} and modeled.^{34,36} We emphasize that these

earlier studies were averaged over the time-profile of the OPO output pulse, whereas we show OPO pulse dynamics in Fig. 9.

5. CONCLUSIONS

The operating characteristics of a narrowband injection-seeded PPKTP OPO pumped at 532 nm by relatively long (27-ns) pulsed SLM radiation have been reported, with particular emphasis on measuring and controlling frequency-chirp effects that arise during the OPO output pulses. This research was preceded by a corresponding study¹¹ of a shorter-pulsed OPO (with 8-ns pump), and a companion paper¹² provides a detailed evaluation of the OH methods that we employ. Whereas previous investigations (e.g., experiments and modeling of a birefringently phase-matched KTP OPO^{15,16}) have examined temporally averaged frequency shifts, our PPKTP OPO studies are able to characterize dynamic frequency perturbations during each OPO pulse.

As in our previous shorter-pulse PPKTP OPO investigations,¹¹ we have reached the important conclusion that it is possible to control the magnitude and the sign of the frequency chirp by adjusting the free-running OPO signal wavelength λ_{free} relative to wavelength λ_s of the TDL injection seeder. The frequency chirp is minimized when these two wavelengths coincide, which corresponds to minimal phase-mismatch Δk . For example, with a PPKTP crystal temperature of 125 °C, yielding $\lambda_{\text{free}} = 841.75$ nm, the frequency chirp was found (Figs. 4 and 5) to be at a minimum with an 841.76-nm TDL-seed wavelength. The smallest mean unsigned overall chirp $\langle |\Delta f_{\text{inst}}| \rangle$ measured (Fig. 6) was 11 ± 3 MHz (evaluated within the arbitrary 10%-intensity range of the OPO signal pulse) or 7 ± 2 MHz (within the more relevant 50%-intensity range).

Our ability to maintain the frequency chirp at ~ 10 MHz or less is at least comparable with that in previously reported^{29–31} chirp-compensated laser systems. We note that chirp-minimization adjustments in our PPKTP OPO system are particularly convenient in that fine control of PPKTP crystal temperature is sufficient to match λ_{free} to a given TDL-seed wavelength (chosen to determine the OPO signal wavelength λ_s). This procedure compares favorably with that for dye-laser systems, in which cumbersome variations of dye concentration are needed to minimize frequency chirp. Given the good chirp reproducibility in our PPKTP OPO system, any residual chirp could be actively compensated by electro-optic phase modulators.⁵

Our long-pulse results contrast with our previous preliminary report¹¹ in which the frequency chirp in a short-pulse injection-seeded PPKTP OPO increases appreciably with pump-laser fluence. We have now found that (within experimental uncertainty as in Figs. 7 and 8) the OPO frequency chirp is insensitive to variations in pump-pulse energy by as much as three times the unseeded threshold, apart from possible complications owing to the onset of partially seeded operation.

Moreover, if the cavity resonance frequency is detuned from its TDL-seed frequency, cavity-pulling frequency

chirp had previously been observed¹¹ with a large value of Δk in the short-pulse PPKTP OPO. However, such effects are no longer evident when Δk is set to zero, as in the present long-pulse PPKTP OPO operating under conditions chosen to minimize chirp.

Our injection-seeded PPKTP OPO system has a sufficiently long output pulse duration (~ 25 ns FWHM) to yield a particularly narrow FT-limited optical bandwidth, measured from OPO pulse time profiles to be ~ 17.5 MHz FWHM. For high-resolution spectroscopic applications this system has the further advantage that the frequency chirp can be maintained at ~ 10 MHz or less and is sufficiently reproducible to facilitate active chirp compensation.

Experiments are under way to extend these investigations to characterize and control frequency chirp in a higher-power OPO-OPA system, with the same long-pulse SLM Nd:YAG laser pumping two or more birefringently phase-matched LiNbO₃ OPA stages to amplify by several orders of magnitude the sub-100- μ J pulse energies of signal output at ~ 842 nm from the present long-pulse PPKTP OPO. We intend in future experiments to add several additional chirp-minimized NLO stages to up-convert tunable, injection-seeded near-IR OPO-OPA signal output into the visible, ultraviolet and VUV regions for high-resolution spectroscopic measurements.

ACKNOWLEDGMENT

We acknowledge financial support from the Australian Research Council.

B. J. Orr's e-mail address is brian.orr@mq.edu.au.

REFERENCES

1. S. D. Bergeson, A. Balakrishnan, K. G. H. Baldwin, T. B. Lucatorto, J. P. Marangos, T. J. McIlrath, T. R. O'Brian, S. L. Rolston, C. J. Sansonetti, J. Wen, N. Westbrook, C. H. Cheng, and E. E. Eyler, "Measurement of the He ground state Lamb shift via the two-photon 1^1S-2^1S transition," *Phys. Rev. Lett.* **80**, 3475-3478 (1998).
2. S. D. Bergeson, A. Balakrishnan, K. G. H. Baldwin, T. B. Lucatorto, J. P. Marangos, T. J. McIlrath, T. R. O'Brian, S. L. Rolston, C. J. Sansonetti, J. Wen, C. H. Cheng, and E. E. Eyler, "Precision spectroscopy in He as a test of QED," *Phys. Scr.* **T83**, 76-82 (1999).
3. S. D. Bergeson, K. G. H. Baldwin, T. B. Lucatorto, T. J. McIlrath, C. H. Cheng, and E. E. Eyler, "Doppler-free two-photon spectroscopy in the vacuum ultraviolet: helium 1^1S-2^1S transition," *J. Opt. Soc. Am. B* **17**, 1599-1606 (2000).
4. J. P. Sprengers, W. Ubachs, K. G. H. Baldwin, B. R. Lewis, and W.-Ü. L. Tchang-Brillet, "Extreme ultraviolet laser excitation of isotopic molecular nitrogen: the dipole-allowed spectrum of $^{15}\text{N}_2$ and $^{14}\text{N}^{15}\text{N}$," *J. Chem. Phys.* **119**, 3160-3172 (2003).
5. K. S. E. Eikema, W. Ubachs, W. Vassen, and W. Hogervorst, "Lamb shift measurement in the 1^1S ground state of helium," *Phys. Rev. A* **55**, 1866-1884 (1996).
6. A. P. Milce and B. J. Orr, "The $\nu_{CC} + 3\nu_{CH}$ rovibrational manifold of acetylene. I. Collision-induced state-to-state transfer kinetics," *J. Chem. Phys.* **106**, 3592-3606 (1997).
7. A. P. Milce and B. J. Orr, "The $\nu_{CC} + 3\nu_{CH}$ rovibrational manifold of acetylene. II. Intramolecular perturbations and symmetry-breaking processes," *J. Chem. Phys.* **112**, 9319-9334 (2000), and references therein.
8. M. A. Payne, A. P. Milce, M. J. Frost, and B. J. Orr, "Symmetry-breaking collisional energy transfer in the $4\nu_{CH}$ rovibrational manifold of acetylene: spectroscopic evidence of a quasi-continuum of background states," *Chem. Phys. Lett.* **324**, 48-56 (2000).
9. G. W. Baxter, M. A. Payne, B. D. W. Austin, C. A. Halloway, J. G. Haub, Y. He, A. P. Milce, J. W. Nibler, and B. J. Orr, "Spectroscopic diagnostics of chemical processes: applications of optical parametric oscillators," *Appl. Phys. B: Lasers Opt.* **71**, 651-663 (2000).
10. M. A. Payne, A. P. Milce, M. J. Frost, and B. J. Orr, "Rovibrational energy transfer in the $4\nu_{CH}$ manifold of acetylene, viewed by IR-UV double resonance spectroscopy. I. Foundation studies at low J ," *J. Phys. Chem.* **107**, 10,759-10,770 (2003).
11. R. T. White, Y. He, B. J. Orr, M. Kono, and K. G. H. Baldwin, "Pulsed injection-seeded optical parametric oscillator with low frequency chirp for high-resolution spectroscopy," *Opt. Lett.* **28**, 1248-1250 (2003).
12. R. T. White, Y. He, B. J. Orr, M. Kono, and K. G. H. Baldwin, "Control of frequency chirp in nanosecond-pulsed laser spectroscopy. 1. Optical-heterodyne chirp analysis techniques," *J. Opt. Soc. Am. B* **21**, 1577-1585 (2004).
13. S. Gangopadhyay, N. Melikechi, and E. E. Eyler, "Optical phase perturbations in nanosecond pulsed amplification and second-harmonic generation," *J. Opt. Soc. Am. B* **11**, 231-241 (1994).
14. P. C. M. Planken, H. J. Bakker, L. Kuipers, and A. Lagendijk, "Frequency chirp in optical parametric amplification with large phase mismatch in noncentrosymmetric crystals," *J. Opt. Soc. Am. B* **7**, 2150-2154 (1990).
15. T. D. Raymond, W. J. Alford, A. V. Smith, and M. S. Bowers, "Frequency shifts in injection-seeded optical parametric oscillators with phase mismatch," *Opt. Lett.* **19**, 1520-1522 (1994).
16. A. V. Smith, W. J. Alford, T. D. Raymond, and M. S. Bowers, "Comparison of a numerical model with measured performance of a seeded, nanosecond KTP optical parametric oscillator," *J. Opt. Soc. Am. B* **12**, 2253-2267 (1995).
17. D. C. Hovde, J. H. Timmermans, G. Scoles, and K. K. Lehmann, "High power injection seeded optical parametric oscillator," *Opt. Commun.* **86**, 294-300 (1991).
18. M. S. Fee, K. Danzmann, and S. Chu, "Optical heterodyne measurement of pulsed lasers: toward high-precision pulsed spectroscopy," *Phys. Rev. A* **45**, 4911-4924 (1992).
19. N. Melikechi, S. Gangopadhyay, and E. E. Eyler, "Phase dynamics in nanosecond pulsed dye laser amplification," *J. Opt. Soc. Am. B* **11**, 2402-2411 (1994).
20. A. E. Siegman, *Lasers* (University Science, Mill Valley, Calif., 1986), p. 332.
21. S. Cussat-Blanc, R. Maleck Rassoul, A. Ivanov, E. Freysz, and A. Ducasse, "Influence of cascading phenomena on a type I second-harmonic wave generated by an intense femtosecond pulse: application to the measurement of the effective second-order coefficient," *Opt. Lett.* **23**, 1585-1587 (1998).
22. M. J. Johnson, Continuum Inc., 3150 Central Expressway, Santa Clara, Calif. 95051 (personal communication, 2002).
23. R. C. Bapna and K. Dasgupta, "Frequency shift in signal and idler gain peaks due to nonlinear refractive index in narrow-band optical parametric oscillators," *J. Mod. Opt.* **49**, 1777-1782 (2002).
24. Y. He, G. W. Baxter, and B. J. Orr, "Locking the cavity of a pulsed periodically poled lithium niobate optical parametric oscillator to the wavelength of a continuous-wave injection seeder by an 'intensity-dip' method," *Rev. Sci. Instrum.* **70**, 3203-3213 (1999).
25. Y. He and B. J. Orr, "Tunable single-mode operation of a pulsed optical parametric oscillator pumped by a multi-mode laser," *Appl. Opt.* **40**, 4836-4848 (2001).
26. G. W. Baxter, J. G. Haub, and B. J. Orr, "Backconversion in a pulsed optical parametric oscillator: evidence from injection-seeded sidebands," *J. Opt. Soc. Am. B* **14**, 2723-2730 (1997).

27. R. DeSalvo, D. J. Hagan, M. Sheik-Bahae, G. Stegeman, and E. W. Van Stryland, "Self-focusing and self-defocusing by cascaded second-order effects in KTP," *Opt. Lett.* **17**, 28–30 (1992).
28. K. S. E. Eikema, W. Ubachs, W. Vassen, and W. Hogervorst, "Precision measurement in helium at 58 nm: ground state Lamb shift and the 1^1S-2^1P transition isotope shift," *Phys. Rev. Lett.* **76**, 1216–1219 (1996).
29. E. E. Eyler, A. Yiannopoulou, S. Gangopadhyay, and N. Melikechi, "Chirp-free nanosecond laser amplifier for precision spectroscopy," *Opt. Lett.* **22**, 49–51 (1997).
30. I. Reinhard, M. Gabrysch, B. Fisher von Weikersthal, K. Jungmann, and G. zu Putlitz, "Measurement and compensation of frequency chirping in pulsed dye laser amplifiers," *Appl. Phys. B: Lasers Opt.* **63**, 467–472 (1996).
31. P. Bakule, P. E. G. Baird, M. G. Boshier, S. L. Cornish, D. F. Heller, K. Jungmann, I. C. Lane, V. Meyer, P. H. G. Sanders, W. T. Toner, M. Towrie, and J. C. Walling, "A chirp-compensated, injection-seeded alexandrite laser," *Appl. Phys. B: Lasers Opt.* **71**, 11–17 (2000).
32. A. V. Smith and M. S. Bowers, "Phase distortions in sum- and difference-frequency mixing in crystals," *J. Opt. Soc. Am. B* **12**, 49–57 (1995).
33. J. C. Barnes, N. P. Barnes, L. G. Wang, and W. Edwards, "Injection seeding. II. Ti:Al₂O₃ experiments," *IEEE J. Quantum Electron.* **29**, 2684–2692 (1993).
34. M. J. Johnson, "Development of pulsed, tunable optical parametric oscillators for spectroscopic applications," Ph.D. dissertation (Macquarie University, Sydney, Australia, 1995).
35. A. Fix, T. Schroder, R. Wallenstein, J. G. Haub, M. J. Johnson, and B. J. Orr, "Tunable β -barium borate optical parametric oscillator: operating characteristics with and without injection seeding," *J. Opt. Soc. Am. B* **10**, 1744–1750 (1993).
36. B. J. Orr, M. J. Johnson, and J. G. Haub, "Spectroscopic applications of tunable optical parametric oscillators," in *Tunable Laser Applications*, F. J. Duarte, ed. (Marcel Dekker, New York, 1995), Chap. 2, pp. 11–83.